International Journal of Innovative
Computing, Information and Control
Volume **9**, Number **4**, April **2013**

ICIC International ©2013 ISSN 1349-4198
pp. 1389–1408

ALTERATION DETECTION AND RECOVERY FOR MEDICAL AND SURVEILLANCE SYSTEMS

Jing-Ming Guo[1], Tsair Kao[2], Chih-Hsien Hsia[1] and Yun-Fu Liu[1]

[1]Multimedia Signal Processing Lab.
Department of Electrical Engineering
National Taiwan University of Science and Technology
No. 43, Sec. 4, Keelung Rd., Taipei 106, Taiwan
jmguo@seed.net.tw; chhsia@ee.tku.edu.tw; yunfuliu@gmail.com

[2]Bioinformation and System Analysis Lab.
Department of Biomedical Engineering
Hungkuang University
No. 34, Chung-Chie Rd., Taichung 43302, Taiwan
tskao@sunrise.hk.edu.tw

Received December 2011; revised April 2012

Abstract. *This study presents two watermarking schemes, namely Halftone Replacement After Watermark Embedding (HRAWE) and Halftone Replacement Before Watermark Embedding (HRBWE), for medical and surveillance systems, respectively. The HRAWE provides better image quality, while HRBWE provides higher robustness to withstand attacks. Two inverse halftoning approaches, Error Diffusion (EDF)-based and Direct Binary Searching (DBS)-based schemes, are also proposed to detect alteration regions and then recover the original image. The EDF-based inverse halftoning has low complexity advantage. Hence, it is mainly used in cooperating with HRBWE for surveillance images to withstand compression or unauthorized modifications. Conversely, the DBS-based inverse halftoning can yield high image quality advantage. Hence, it is mainly used in cooperating with HRAWE for medical images to detect and recover unauthorized modifications. Both of the approaches are proved to yield excellent performance with extensive experimental results.*

Keywords: Authentication, Direct binary search, Digital halftoning, Digital watermarking, Error diffusion, Inverse halftoning, Ordered dithering

1. **Introduction.** Nowadays, numerous of digital multimedia data have been widely spread through Internet. The unauthorized distribution of multimedia data becomes much easier. Consequently, the copyright protection [1] and authentication [2] raise more and more attention. Among the multimedia security schemes, the robust watermarking is a powerful mechanism to address the copyright protection issue. The embedded copyright information in multimedia can be extracted to identify the owner's license information and track illegal copies. Conversely, the watermarking should be fragile in content authentication application, so that it can detect the alterations of the protected contents.

In general, the watermarking schemes can be mainly classified into two parts: Spatial domain [3-5] and transform domain [6-16,18-20,22-24]. The spatial domain watermarking generally has lower complexity but lower robustness to withstand attacks. Conversely, the transform domain watermarking normally has higher robustness but higher complexity. According to the additional information available in the decoder, these methods can also be classified into three categories: The first category is non-blind watermarking [6-11] which needs the original image to decode the watermark. The second category is blind

watermarking [12-16], in which the watermark can be decoded without the host image. The third is the semi-blind watermarking [18-20] which requires the secret keys and the original watermark. The details of these categories are discussed as below.

Spatial domain watermarking approaches are mostly utilized in early history of watermarking development. Those methods include: Watermarking by slightly modifying the intensity of random selected image pixels in spatial domain [3]; using the spatial-domain bit-string embedding technique to modulate the image signal with random zero-mean patches at random locations [4], and embedding the watermark in the least significant bits (LSBs) of image pixels [5].

Transform domain techniques can distribute a watermark into a wide range of pixels by simply modifying coefficients in transform domain. Hence, the embedded images are more robust to against attacks. The related researches include: Using the concept of spread spectrum to embedded watermark in transform domain (DCT or FFT), where the Gaussian distributed sequence is embedded to resemble the nature watermarks [6]. The spread spectrum scheme was later generalized to embed watermark in wavelet coefficients of images and video [7]. Hsu and Wu [8] proposed a DCT-based watermarking to embed visually recognizable patterns in the middle frequency coefficients. Huang *et al.* [9] embedded watermark by modifying the DC components to provide higher robustness. Lu *et al.* [10] proposed the cocktail watermarking technique, where the complementary modulation rules are used in wavelet transform domain for watermark embedding. If the attack generates the positive distortion, the negative one will still survive, and vice versa. In [24], the feature point watermarking synchronization and the wavelet transform-based watermarking embedding/extraction are proposed. Wavelet-domain watermarking is robust to signal processing attacks and watermarking synchronization gets rid of the effect of geometric attacks. However, it cannot provide the additional recovery capability to against compression and cropping attacks. Conversely, the proposed scheme can provide alteration detection and further recovery features.

In blind watermarking approaches, the original image and watermark are not required in the decoder. Those methods in the literature include: Lu and Liao [12] extended the cocktail watermarking to be a blind multipurpose watermarking system which can detect malicious modifications. Khelifi *et al.* [13] divided the image into non-overlapped blocks, using JND-based classifier to classify blocks into two parts: uniform and non-uniform. The Neyman-Pearson criterion was used to extract watermark. Wang *et al.* [14] embedded watermark in significant coefficients of wavelet domain, and then employed the trained neural network to exactly recover the watermark. Inoue *et al.* [15] proposed two methods to classify the wavelet coefficients into significant and insignificant two parts, and then embedded watermark by EZW algorithm [17]. The position of zerotree's root is then used to detect the watermark.

Many semi-blind watermark techniques are also addressed in the literature. Huo and Guo [18] embedded watermark into significant triplet wavelet coefficients in the lowest three detail subbands, and the selected significant triplet positions are adopted for extracting watermark. Solachidis and Pitas [19] used the watermark possesses circular symmetry which is embedded in a ring of the DFT domain. Correlation between the possibly watermarked coefficients and watermark is used for watermark detection. Al-Khassaweneh and Aviyente [20] presented a semi-blind watermark extraction algorithm, where the threshold for a given probability of false alarm is derived. The modified coefficients are located according to the given key.

The watermarking approaches introduced above cannot recover the original host image when an embedded image is attacked. For this, the digital halftoning is adopted to solve this problem. Digital halftoning [21] is to render multi-tone images using only two-tone

elements. A halftone image resembles the original grayscale image when viewed at a proper distance due to the lowpass nature of the human visual systems. Hence, it is adopted in this study as a tool for recovering the original host image by cooperating a trained LMS filter when the embedded image is suffered from alterations. Many halftoning methods have been developed, including ordered dithering, error diffusion [22,33], dot diffusion [34,35], and iteration-based method [36-40]. Among these, error diffusion offers good visual quality and reasonable computational complexity, and iteration-based method provides best image quality and highest complexity. Both of the error diffusion and iteration-based methods are adopted in this work to address the issue of image recovery.

In this paper, two different types of watermarking approaches are proposed to adapt for different applications. The main goal is to be applied in medical and surveillance systems. Hence, throughout this study, two related attacks, cropping and compression, are taken into consideration. The first method, namely Halftone Replacement After Watermark Embedding (HRAWE), is used for applications without compression attack, such as medical imaging system. The second method, namely Halftone Replacement Before Watermark Embedding (HRBWE), is used for application with compression attack, such as surveillance system. Both of the proposed schemes can be used to detect alteration and recover the original image. The reason that we dedicate on the two applications is their special requirements in practice: The medical system demands high image quality, and the surveillance system requires real-time low complexity and robustness for reasonable compression attack. The watermarking on both applications requires another capability of alteration region detection and recovery. As documented in the experimental results, the proposed HRAWE provides good image quality, and HRBWE provides good robustness to withstand attacks.

The rest of this work is organized as follows. Section 2 provides an overview of digital halftoning and inverse halftoning. Section 3 introduces the proposed HRAWE and HRBWE schemes. Section 4 shows the experimental results, and Section 5 draws conclusions.

2. **Overview of Digital Halftoning and Inverse Halftoning.**

In this section, the two well-known halftoning methods, Error Diffusion (EDF) and Direct Binary Searching (DBS), and the corresponding inverse halftoning are introduced. The EDF is an efficient approach to obtain a good halftone image, and DBS is an iteration-based approach to obtain an optimized halftone result. Both approaches are adopted for alteration detection and image recovery after the embedded image is undergone attack. The EDF is mainly used in surveillance system for its real-time requirement. Conversely, the DBS is used in medical system for its high quality requirement. In general, a halftone image is in binary fashion, black or white. The inverse halftoning is to reconstruct an approximate grayscale version of the original image, and thus it can provide better knowledge of the original grayscale image.

2.1. **Error diffusion (EDF).**

Floyd and Steinberg [25] proposed a reasonable computational halftoning with good image quality and high spatial resolution, named error diffusion, by quantizing each pixel according to a statistical analysis of the input pixel and its neighbors, leading to a stochastic arrangement of the printed dots. In addition, when it comes to display color works, this technique eliminates the occurrence of the moiré effect which is produced by superimposing two or more halftone patterns of different color channels. In the past few years, the error diffusion had great progress in printing industry, which included the following studies: Applying adaptive error kernels to distribute errors to three instead of four neighbors [26] to decrease the computational

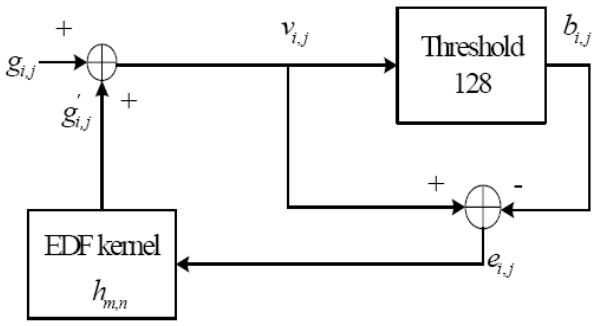

FIGURE 1. Standard error diffusion flow chart

complexity and eliminate the worm effect inherently existing in halftone patterns, and the concept of using green-noise halftoning algorithm to produce patterns with adjustable coarseness which can be tuned to adapt to the reliability of a given printer to produce dots consistently [27-33].

Figure 1 shows the standard EDF flow chart. The variable $g_{i,j}$ denotes the current input pixel value and $g'_{i,j}$ denotes the diffused error sum added up from the neighboring processed pixels. The variable $b_{i,j}$ denotes the binary output in position (i,j), and the error kernel $h_{m,n}$ denotes the error kernel used to diffuse the error caused by the difference, $e_{i,j}$, between the output binary value and the input gray level value. The variable $v_{i,j}$ is the modified gray output. The relationships among $b_{i,j}$, $v_{i,j}$, and $e_{i,j}$ are organized as

$$v_{i,j} = g_{i,j} + g'_{i,j}, \text{ where } g'_{i,j} = \sum_{m=0}^{2} \sum_{n=-2}^{2} e_{i+m,j+n} \times h_{m,n} \tag{1}$$

$$e_{i,j} = v_{i,j} - b_{i,j}, \text{ where } b_{i,j} = \begin{cases} 0 & \text{if } v_{i,j} < 128 \\ 255 & \text{if } v_{i,j} \geq 128 \end{cases} \tag{2}$$

Herein, we numerically define 0 and 255 as a black and while pixel, respectively.

2.2. **Direct binary search (DBS).** The DBS is first introduced by Analoui and Allebach [36], where the optimized halftone patterns are generated with iteration-based method. Suppose the original grayscale image is of size $P \times Q$, the iterative reconstruction procedure is described as follows:

1) Set $b_{i,j}^{(1)} = 0$, $i,j \in P \times Q$

2) $b_{i,j}^{(k)} = \{b_{i,j}^{(k-1)} | b_{i,j}^{(k-1)} \text{minimize} | g_{i,j} - \sum_{m,n \in R} \sum w_{m,n} b_{i+m,j+n}^{(k-1)} |$, $b_{i,j}^{(k-1)}$ toggles between 0 and 1 or swaps with its eight neighbors$\}$

3) $E_{total}^{(k)} = \sum_{i,j \in P \times Q} \sum \left| g_{i,j} - \sum_{m,n \in R} \sum w_{m,n} b_{i+m,j+n}^{(k)} \right|$

4) If $E_{total}^{(k)} = E_{total}^{(k-1)}$, stop, otherwise go to Step 2 and continue

where $b_{i,j}^{(1)}$ denotes the initial binary image, which can be initialized as whole black; $g_{i,j}$ and $b_{i,j}$ denote the original grayscale image and the DBS halftone image, respectively, and $w_{m,n}$ denotes the HVS filter adopted in [36], where the support region is denoted as R. Each pixel is toggled or swapped with its eight neighbors to generate 10 candidates (including the original one). The one minimized the cost function given in Step 2 is maintained. This procedure is iteratively conducted until the DBS image is convergent without any change as defined in Step 4.

2.3. **Inverse halftoning.** In this study, the LMS-trained filter is used to perform inverse halftoning. The LMS-based halftone technique can be divided into two steps. The first step is the training procedure to derive the optimized coefficients for the LMS filter, and the second step is to use the trained LMS filter to obtain the corresponding inverse halftone image from a halftone image. The LMS training phase can be mathematically described as

$$\hat{g}_{i,j} = \sum_{m,n \in R} \sum w_{m,n} h_{i+m,j+n}, \tag{3}$$

$$e_{i,j}^2 = (g_{i,j} - \hat{g}_{i,j})^2, \tag{4}$$

$$\frac{\partial e_{i,j}^2}{\partial w_{m,n}} = -2e_{i,j} h_{i+m,j+n}, \tag{5}$$

$$\begin{cases} \text{if } w_{m,n} > w_{m,n,opt},\ slope > 0,\ w_{m,n} \text{ should be decreased} \\ \text{if } w_{m,n} < w_{m,n,opt},\ slope < 0,\ w_{m,n} \text{ should be increased,} \end{cases} \tag{6}$$

$$w_{m,n}^{(k+1)} = w_{m,n}^k + \mu e_{i,j} h_{i+m,j+n}, \tag{7}$$

where $\hat{g}_{i,j}$ denotes the reconstructed grayscale pixel at position (i, j); R denotes the support region of the LMS filter. (e.g., 5×5 or 7×7); $w_{i,j}$ denotes the LMS coefficient at position (i, j); $w_{i,j,opt}$ denotes the optimum LMS coefficient; $e_{i,j}^2$ denotes the MSE between $g_{i,j}$ and $\hat{g}_{i,j}$; μ denotes the adjusting parameter used to control the convergent speed of the LMS optimum procedure, with the value set to 10^{-5} in this study. Here we conduct a series of experiments to demonstrate the reason we choose this number: Eight training images are involved in filter reconstructing process, including Lena, Mandrill, Peppers, Milk, Airplane, Earth, Lake, and Tiffany images. Four kinds of different original halftone techniques, including DBS, EDF, dispersed-dot dithering, and clustered-dot dithering, are employed. Four different LMS filter of sizes 3×3, 5×5, 7×7, 9×9, and parameter μ of

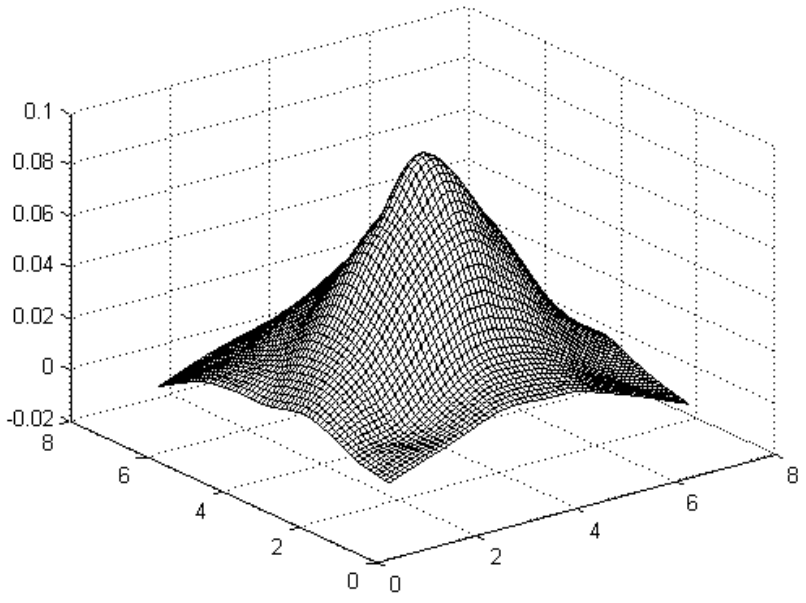

FIGURE 2. LMS-trained human visual filter (7×7)

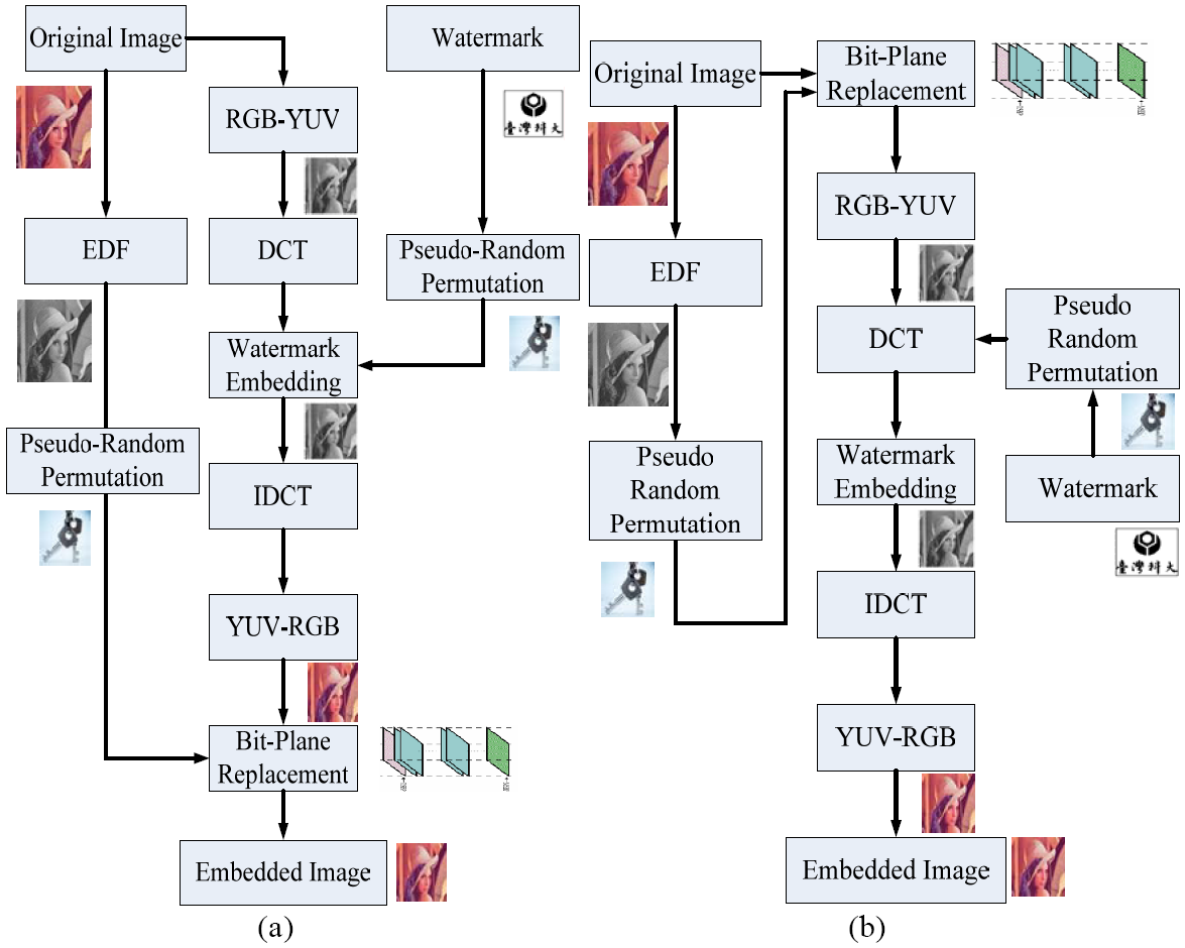

FIGURE 3. Two proposed watermarking conceptual diagrams: (a) HRAWE, (b) HRBWE

three different values, 10^{-4}, 10^{-5}, and 10^{-6}, are also tested. The absolute overall change of the LMS filter in each training iteration is defined as follows:

$$change(k) = abs\left(\sum_{m,n\in R}\sum w_{m,n}^{(k)} - w_{m,n}^{(k-1)}\right), \tag{8}$$

where k represents the number of iteration. The smaller the value of $change(k)$ is, the closer it approximates the convergence. From the experimental results, the parameter μ with value 10^{-6} takes copious time to converge, which is even longer as the filter size grows up. Conversely, the parameter μ with value 10^{-5} gives reasonable convergent speed, usually within five iteration times, and the parameter μ with value 10^{-4} achieves highest convergent speed. However, it cannot yield better reconstructed halftone quality than the filter obtained from parameter μ with values 10^{-5} and 10^{-6}. In Figure 6, various reconstructed mandrill halftone results are demonstrated with different combination of LMS filter size and parameter μ. Herein, eight tested images are also employed for reconstructing halftone images using LMS filter of different sizes. We found that the LMS filter of size 3×3 leads to artifacts similar to false contour. On the other hand, filter of size 9×9 or larger simply offer little benefit in quality, but substantially increase the computational complexity. Consequently, the filter sizes of 5×5 or 7×7 are more suited for reconstructing the halftone images. Of these, the filter of size 7×7 generally gives much sharper and higher halftone quality than that of the filter of size 5×5, although it

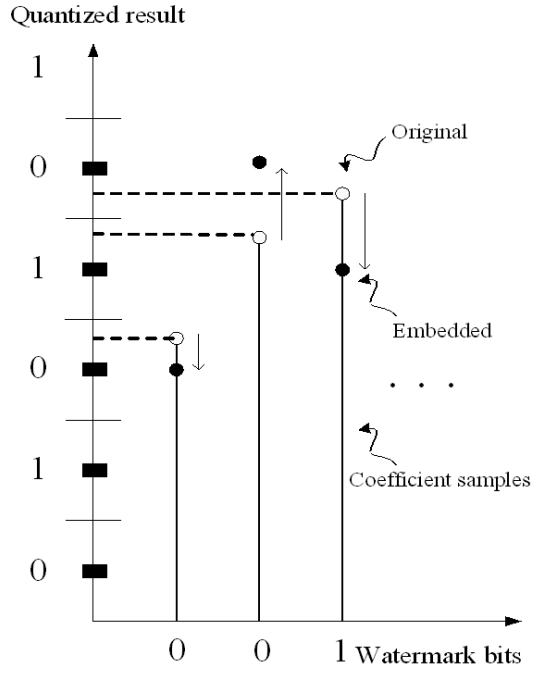

FIGURE 4. Example of embedding 001 watermark bits into three coefficients in DCT domain

has higher computational complexity. Hence, in this study we choose filter of size 7×7, as shown in Figure 2, for the following inverse halftoning reconstruction. The mathematical equation is given in Equation (3). Notably, the filter has the basic characteristics of human visual system:

1) The diagonal (45°) has less sensitivity (lower values) than vertical and horizontal directions.

2) The center has the highest sensitivity and decay with the increasing distance to center.

3. MRAWE and HRBWE.

3.1. **Watermark embedding.** Two different types of watermarking approaches are proposed to adapt for different applications. The first method, namely Halftone Replacement After Watermark Embedding (HRAWE), is used for applications without compression attack, such as medical imaging system. The second method, namely Halftone Replacement Before Watermark Embedding (HRBWE), is used for applications possibly undergone compression attack, such as surveillance system. Both of the proposed schemes can be used to detect alteration and then further recover the original image. The two encoding procedures, as illustrated in Figure 3, are introduced as below:

1. HRAWE:

1) Transform the original image from RGB color space to YUV color space.

2) The Y component $g_{i,j}$ is divided into blocks of size M×N, then each block is transformed with DCT to form $g^T_{i,j}$.

3) The original watermark $w_{i,j}$ is permutated with a pseudo random key to form $w^P_{i,j}$ to increase the security.

4) Suppose the image is of size $P \times Q$, and the watermark is of size $\frac{P}{M} \times \frac{Q}{N}$, then each watermark bit is embedded into a block of the host image. The magnitude of the coefficients in DCT domain are quantized to odd and even steps, where odd steps map to 0

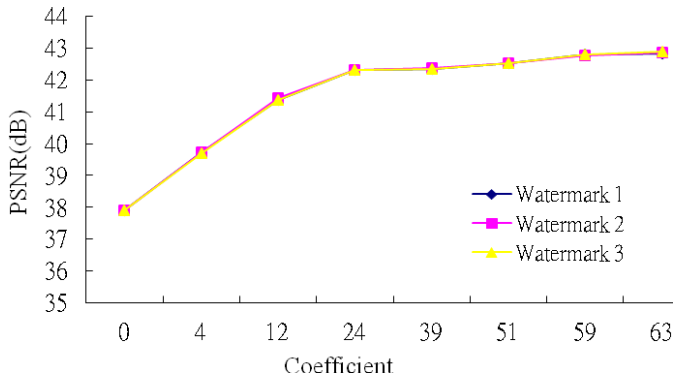

FIGURE 5. Average PSNR using after watermark is embedded

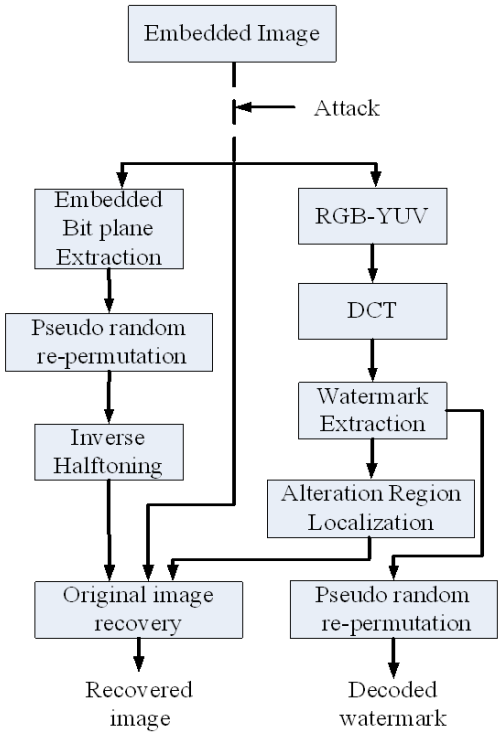

FIGURE 6. Conceptual diagram of watermark decoding and original image recovery

and even sections map to 1. The pseudo random permutated watermark $w_{i,j}^P$ is embedded into $g_{i,j}^T$ to form $\hat{g}_{i,j}^T$ by modifying the coefficient to the nearest neighbor step with the same attribute, 0 or 1, as the watermark bit. Figure 4 shows an example of embedding 001 watermark bits into three coefficients. To determine the best embedded position in a block, each position is addressed with a number in zig-zag fashion from 0 to 63. According to the observation from experimental results, the diagonal coefficients are the best candidates to avoid horizontal or vertical artifacts. To maintain robustness requirement against compression attack, the coefficient with index 4 is employed for embedding watermark in this study. Figure 5 shows the average PSNR with five host images and three different watermarks when different diagonal coefficients are used for embedding.

5) The inverse DCT is applied to the embedded coefficients $\hat{g}_{i,j}^T$ to form the spatial domain information $\hat{g}_{i,j}$.

6) Transform the YUV color space to RGB color space.

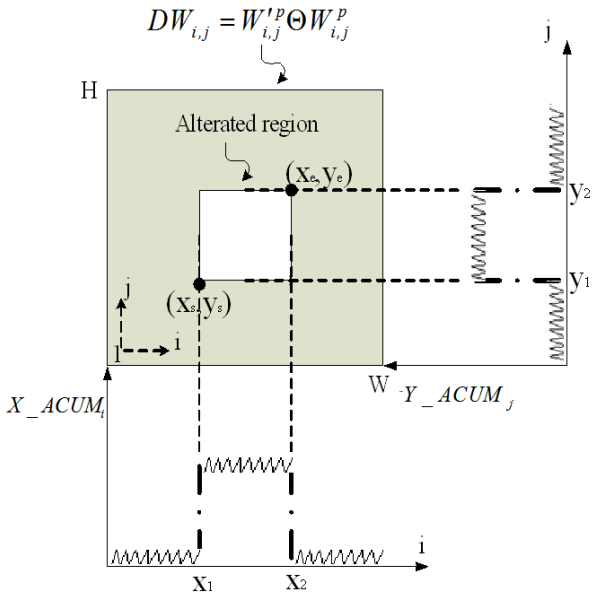

FIGURE 7. Alteration region localization

7) The halftoning is applied to the three color spaces, R-G-B, of the original host image, and the three halftone images are then used to replace the LSB planes (bit plane 0) of the three embedded color spaces. The replaced halftone images are used for recover the original information when encounter unauthorized alterations.

2. HRBWE:

The main difference between HRAWE and HRBWE is in Step 7, where HRBWE replaces the bit plane before RGB to YUV color space transformation. The HRBWE is mainly used for withstanding compression attack. As illustrated in Figure 3(b), the halftone image in HRBWE is distorted by the watermark embedding procedure. Hence, it is designed to adopt the bit plane 3 for halftone image substitution to provide a trade-off performance between robustness and image quality.

3.2. **Watermark decoding.** The watermark decoding procedure involves the following steps, which is illustrated in Figure 6:

1) Transform the embedded image from RGB color space to YUV color space.

2) The Y component is further processed with DCT.

3) The permutated watermark is extracted according to the coefficient with zig-zag index 4 locates in which quantized step, 0 or 1.

4) The pseudo random key is used to obtain the decoded watermark.

3.3. **Alteration region localization and original image recovery.** Suppose the variables $w^P_{i,j}$ and $w'^P_{i,j}$ denote the embedded permutated watermark and the decoded permutated watermark, respectively. Let the difference watermark be $DW = w'^P_{i,j} \Theta w^P_{i,j}$, where Θ denotes the exclusive-OR operation; the alteration region localization procedure is organized as below.

Figure 7 shows the conceptual diagram of the alteration region localization, where X_ACUM_i and Y_ACUM_j denote the accumulated difference number along i and j-axes.

The two variables are defined below:

$$X\_ACUM_i = \sum_{j=1}^{H} DW_{ij} \tag{9}$$

$$Y\_ACUM_j = \sum_{i=1}^{W} DW_{ij} \tag{10}$$

where the variables H and W denote the height and width of the difference watermark. The successive difference of the X_ACUM_i and Y_ACUM_j are defined below.

$$X\_ACUM\_DIFF_i = X\_ACUM_i - X\_ACUM_{i-1} | i = 2, \ldots, W \tag{11}$$

$$Y\_ACUM\_DIFF_j = Y\_ACUM_j - Y\_ACUM_{j-1} | j = 2, \ldots, H \tag{12}$$

The two variables defined above are used to determine the start point (x_s, y_s) and end point (x_e, y_e) of the rapid-varying region, as given by

$$\begin{aligned}(x_s, y_s) = (&\max\{X\_ACUM\_DIFF_i | i = 2, \ldots, W\}, \\ &\max\{Y\_ACUM\_DIFF_j | j = 2, \ldots, H\})\end{aligned} \tag{13}$$

$$\begin{aligned}(x_e, y_e) = (&\min\{X\_ACUM\_DIFF_{i-1} | i = 2, \ldots, W\}, \\ &\min\{Y\_ACUM\_DIFF_{j-1} | j = 2, \ldots, H\})\end{aligned} \tag{14}$$

The corresponding alteration region in embedded image is the rectangular area surround by the two coordinates, (Nx_s, My_s) and (Nx_e, My_e), where $M \times N$ denotes the DCT block size.

The original image recovery involves the following steps, which is illustrated on the left hand side of Figure 6:

1) The halftone replaced bit planes of the RGB three color spaces are extracted from the embedded image, which corresponds to the permutated halftones of the original image.

2) The pseudo random key is used to reconstruct the original halftones of the original image.

3) The inverse halftoning introduced in Section 2.3 is applied to reconstruct the grayscale information of the RGB three color spaces.

4) The alteration localized region is replaced with the inverse halftone images.

4. **Experimental Results.** In this section, extensive experiments are conducted with the proposed two watermarking schemes, HRAWE and HRBWE, to demonstrate the performance. Figures 8(a)-8(g) show the seven test images of size 720×576, and Figures 8(h)-8(j) show the three test watermarks of size 90×72. In addition, in the following experiments, the DCT coefficient with the index 4 is adopted for watermark embedding as discussed in Section 3.1.

Figure 9 shows the image quality comparison between the proposed EDF and DBS inverse halftoning results. Supposing an image is of size PxQ, the definition of PSNR is given below

$$PSNR = 10 \log_{10} \frac{255^2 \times P \times Q}{\sum_{i=1}^{P} \sum_{j=1}^{Q} \left[\sum_{(m,n) \in W} w_{m,n} (g_{i+m,j+n} - g'_{i+m,j+n}) \right]^2}, \tag{15}$$

where $g_{i,j}$ and $g'_{i,j}$ denote the original image and the inverse halftone image, respectively, and $w_{i,j}$ denotes the weights of a human visual system like low-pass filter to simulate the nature of human visual system. In this study, the trained LMS filters of different sizes as discussed in Section 2.3 are adopted for this evaluation. To provide an objective

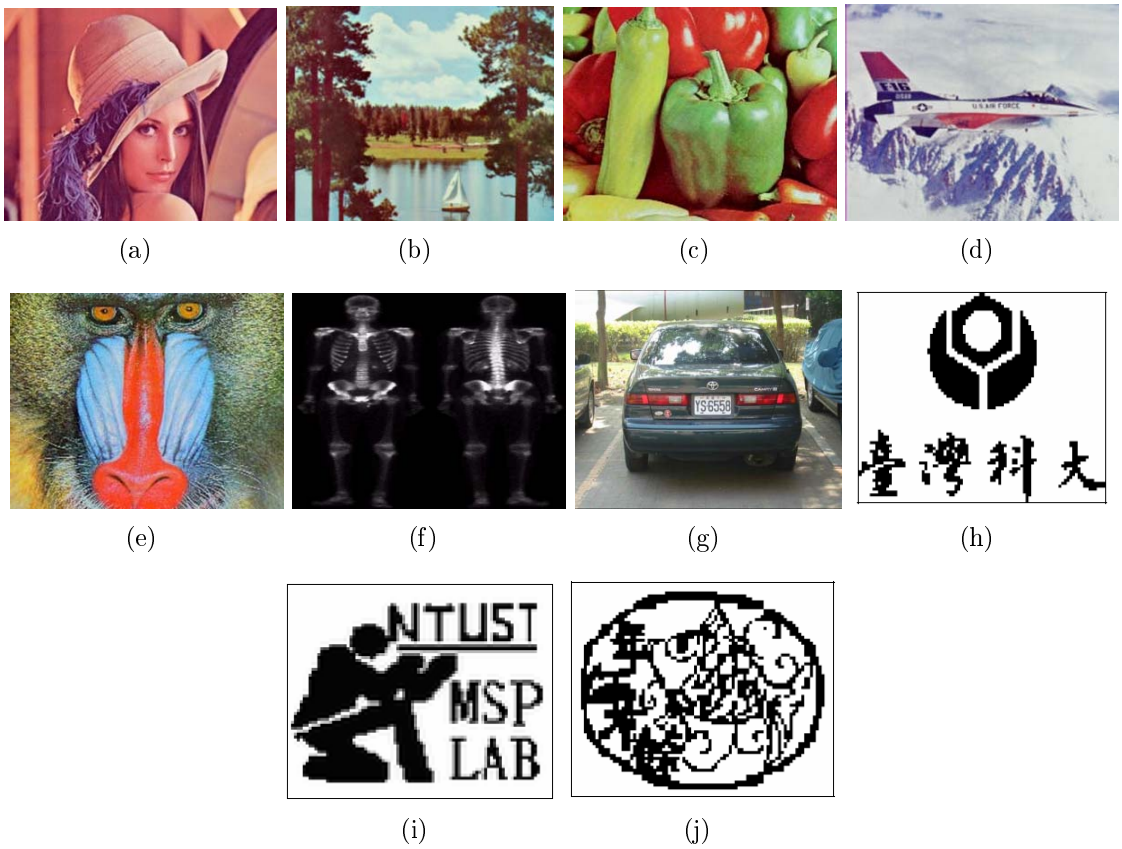

FIGURE 8. Test images and watermarks: (a)-(g) test images of size 720×576; (h)-(j) test watermarks of size 90×72

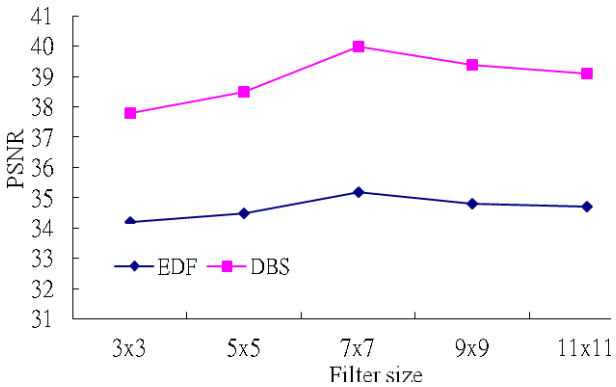

FIGURE 9. Average image quality comparison between the proposed EDF and DBS inverse halftoning results

evaluation, five different filter sizes are tested in this experiment. Apparently, the DBS outperforms EDF under all filter sizes. However, the DBS is time-consuming with its iteration-based reconstruction fashion. Hence, the EDF inverse halftoning is a good solution for real-time application, such as surveillance system, and the DBS inverse halftoning is better suited for high quality oriented application, such as medical imaging system. Basically, the changes of filter sizes for estimating the PSNR do not affect the evaluation, thus the filter size 7×7 is selected for the following experiments.

In this work, we rather choose two most possible attacks, compression and cropping related to the surveillance and medical applications. In fact, the cropping attack is same

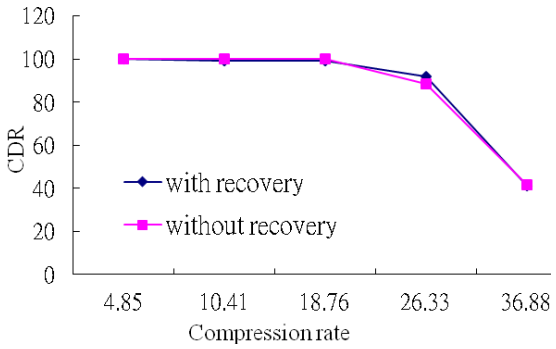

FIGURE 10. Average CDR of the decoded watermark versus compression rates with or without recovery function using HRAWE

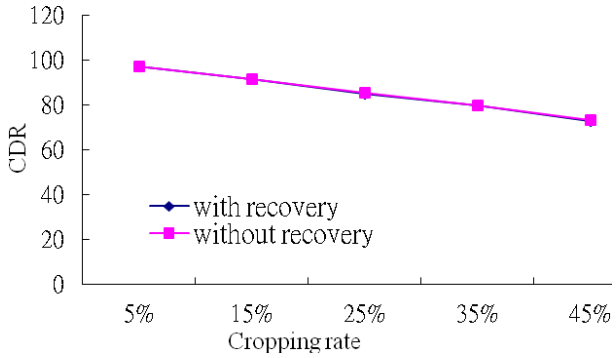

FIGURE 11. Average CDR of the decoded watermark versus cropping rates with or without recovery function using HRAWE

as most replacement attacks, such as replacing one face in an image with another face. Since the recovery function (inverse halftoning) can be disabled during the watermark embedding, the Correct Decoding Rate (CDR) of the decoded watermark versus compression rates and cropping rates with or without recovery function are shown in Figures 10 and 11, where the bit plane 0 is selected. It is clear that the additional recovery function barely affect the performance in CDR. Suppose the watermark is of size $\frac{P}{M} \times \frac{Q}{N}$. The definition of CDR is given below, where the notations are defined the same as above.

$$CDR = \frac{\sum_{i=1}^{P/M} \sum_{j=1}^{Q/N} \overline{W'_{i,j}{}^{P} \Theta W^{P}_{i,j}}}{P/M \times Q/N}, \tag{16}$$

Figures 12 and 13 show the average recovered image quality under cropping and compression attacks, respectively, using the EDF inverse halftoning. The results show that the HRAWE provides better recovery image quality than that of the HRBWE, since the halftone image in HRBWE is somewhat damaged by watermark embedding procedure as shown in Figure 3(b). Herein, the halftone image is embedded in bit plane 0 and 3 for HRAWE and HRBWE, respectively. Figures 14 and 15 show the average recovered image quality under cropping and compression attacks, respectively, using the DBS inverse halftoning. Both of the results are superior to the results shown in Figures 12 and 13. Hence, if the complexity is not a critical issue in application, such as medical system, the DBS inverse halftoning is a good solution in image recovery.

Figures 16 and 17 show the average CDR of the decoded watermark under cropping and compression attacks, using EDF inverse halftoning. Since the the halftone image is embedded in bit plane 0 and 3 for HRAWE and HRBWE, respectively, the HRBWE

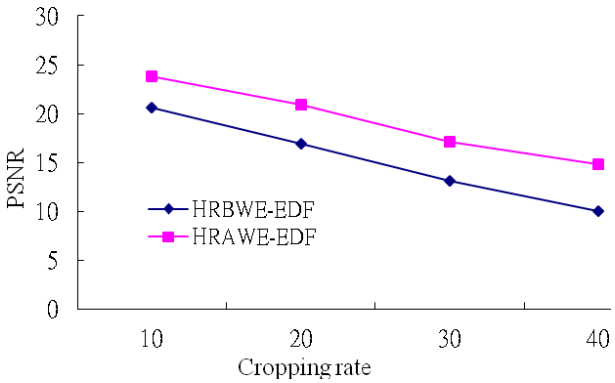

FIGURE 12. Average recovered image quality under cropping attack using EDF inverse halftoning

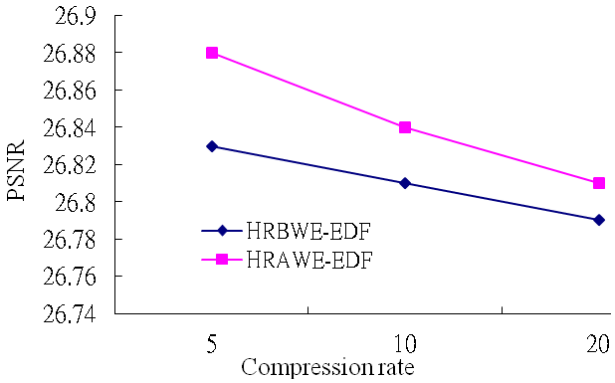

FIGURE 13. Average recovered image quality under compression attack using EDF inverse halftoning

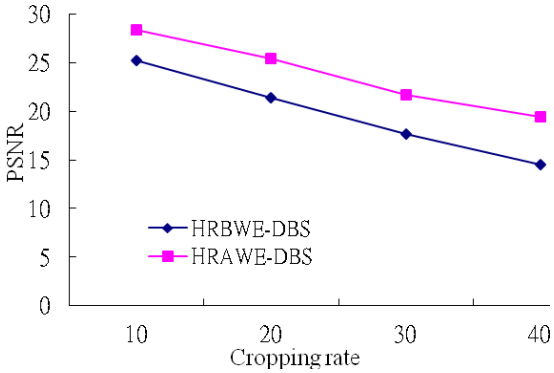

FIGURE 14. Average recovered image quality under cropping attack using DBS inverse halftoning

provides much better robustness than that of the HRAWE. Moreover, the HRBWE is insensitive to compression rate, since the low frequency DCT coefficient with index 4 is employed for embedding.

Figures 18 and 19 show the average recovered image PSNR vs. halftone replaced bit plane number by fixing cropping rate at 20% and compression rate at 10, respectively. Both of the results adopt EDF inverse halftoning. In both cases, the HRAWE are better than HRBWE, although the HRAWE is only higher than HRBWE by 0.02dB in Figure 19. Figures 20 and 21 show the average recovered image PSNR vs. halftone replaced bit plane number, using DBS inverse halftoning. The recovered image quality are better than

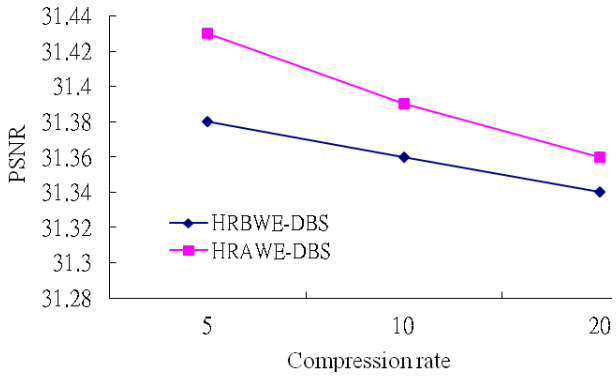

FIGURE 15. Average recovered image quality under compression attack using DBS inverse halftoning

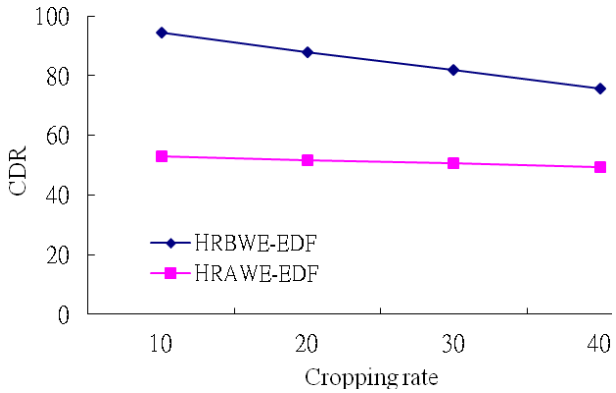

FIGURE 16. Average decoded watermark CDR under cropping attack using EDF inverse halftoning

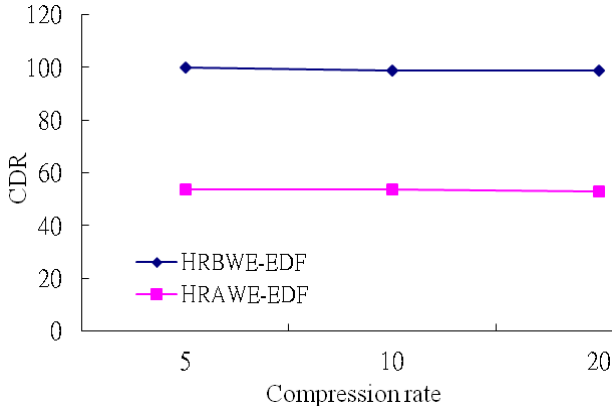

FIGURE 17. Average decoded watermark CDR under compression attack using EDF inverse halftoning

that of Figures 18 and 19. Again, DBS is proved to be better than EDF in image quality regard.

Figures 22 and 23 show the average decoded watermark CDR vs. halftone replaced bit plane number by fixing cropping rate at 20% and compression rate at 10, respectively, using EDF inverse halftoning. The results show that the HRBWE has little effect by cropping and compression attacks. In HRAWE, the bit plane is replaced with its halftone image after the watermark is embedded, the watermark information is reduced when a

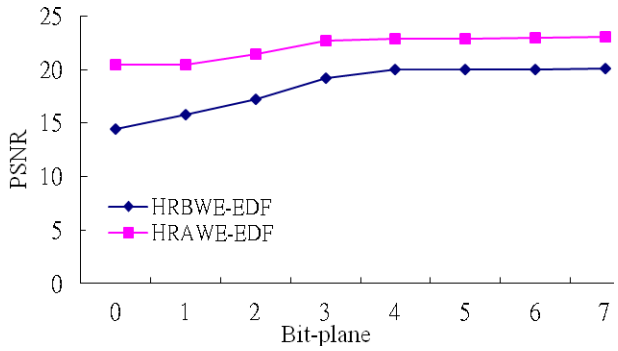

FIGURE 18. Average recovered image PSNR vs. halftone replaced bit plane number by fixing cropping rate at 20% (EDF inverse halftoning)

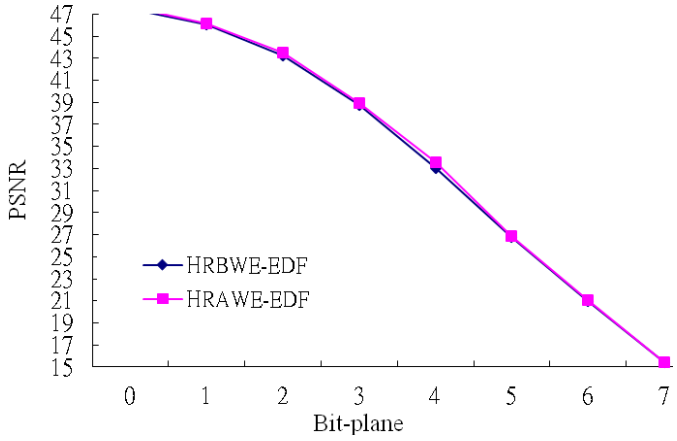

FIGURE 19. Average recovered image PSNR vs. halftone replaced bit plane number by fixing JPEG compression rate at 10 (EDF inverse halftoning)

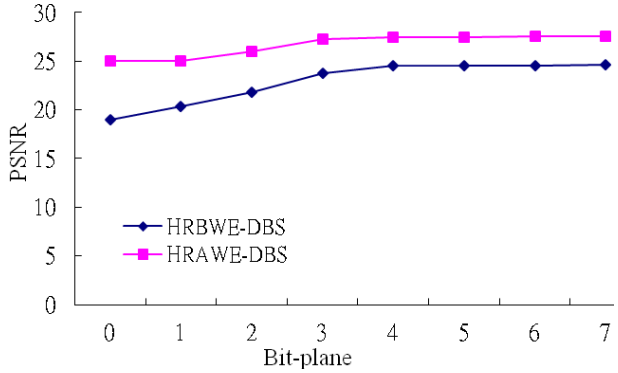

FIGURE 20. Average PSNR vs. replaced bit plane by fixing cropping rate at 20% (DBS inverse halftoning)

higher bit plane is replaced with its halftone image. Since the image recovered function is not discussed here, the DBS invese halftoning is not included for comparison.

In this work, we rather choose two most possible attacks, compression and cropping related to the surveillance and medical applications. Figures 12 and 15 show the average recovered image quality under cropping and compression attacks, respectively, using the EDF and DBS inverse halftoning. As it can be seen from the results, if the complexity is not a critical issue in application, such as medical system, the DBS inverse halftoning is a good solution in image recovery. Two watermarking approaches, HRAWE and HRBWE

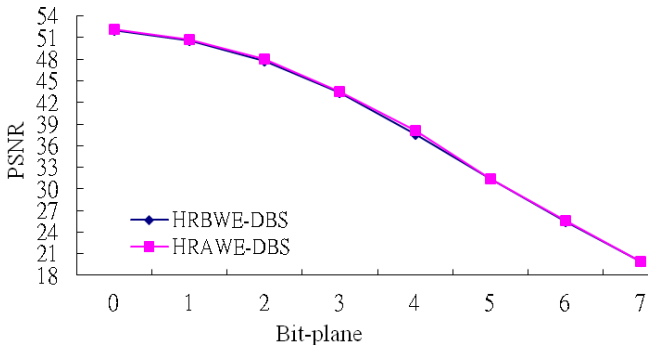

FIGURE 21. Average PSNR vs. replaced bit plane by fixing JPEG compression rate at 10 (DBS inverse halftoning)

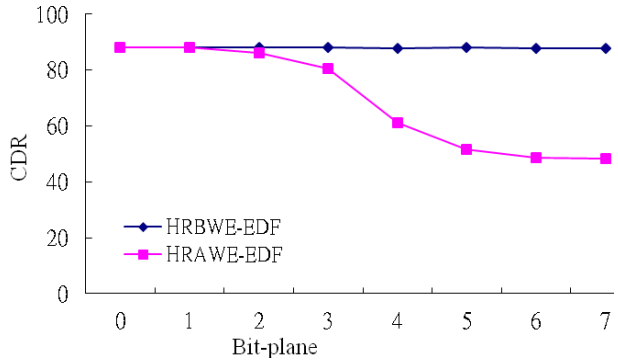

FIGURE 22. Average decoded watermark CDR vs. halftone replaced bit plane number by fixing cropping rate at 20% using EDF inverse halftoning

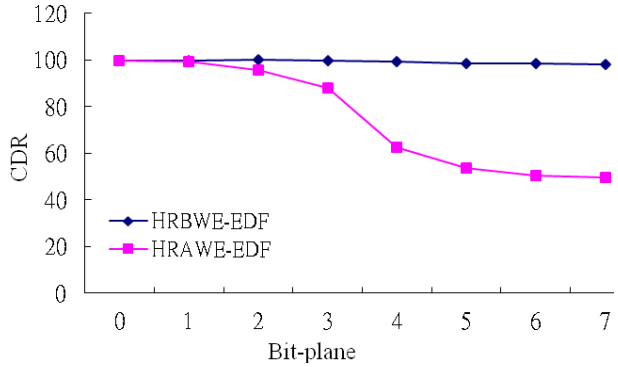

FIGURE 23. Average decoded watermark CDR vs. halftone replaced bit plane number by fixing JPEG compression rate at 10 using EDF inverse halftoning

are proposed to provide alteration detection and image recovery features. The main goal is to be applied in medical and surveillance systems, respectively. Hence, throughout this study, two related attacks, cropping and compression, are taken into consideration. The HRAWE provides better image quality, while HRBWE provides higher robustness to withstand attacks. Moreover, two inverse halftoning approaches, EDF-based and DBS-based, are also proposed to detect alteration region and then recover the original image. As documented in the experimental results, the proposed HRAWE provides good image quality, and HRBWE provides good robustness to withstand attacks, as shown in Figures 24 and 25. Figures 24 and 25 show a practical medical application using HRAWE and a practical surveillance application using HRBWE, respectively. In which, the bit planes for

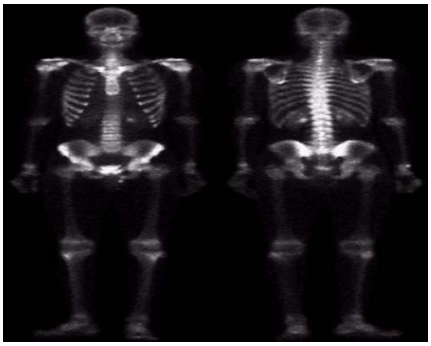

(a)

(b)

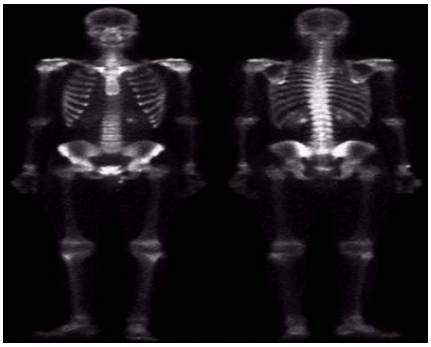

(c)

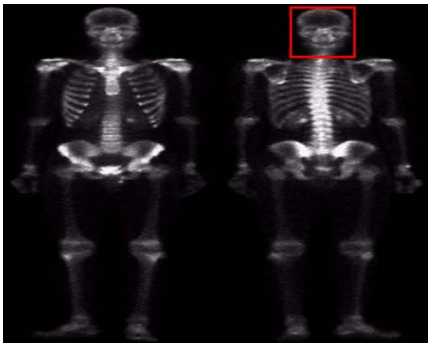

(d)

(e)

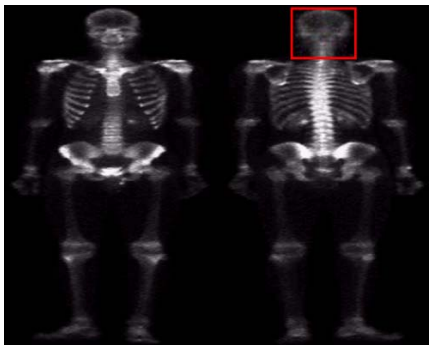

(f)

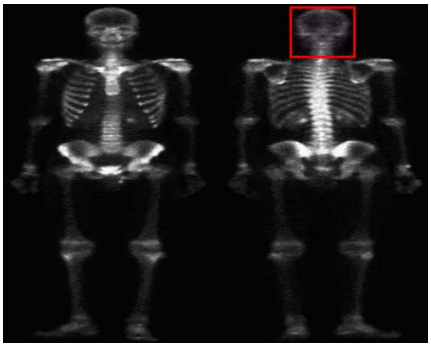

(g)

PSNR	Decoded Modified Coordination		CDR
EDF 51.11 (dB)	Alteration position	Detected position	99.12 %
DBS 55.66 (dB)	(Nx_s, My_s) = (482, 487) (Nx_e, My_e) = (565, 591)	(Nx_s, My_s) = (488, 488) (Nx_e, My_e) = (568, 592)	

(h)

FIGURE 24. Medical application with HRAWE. (a) Original host image. (b) Original watermark. (c) Embedded result. (d) Alterated and detected result (in red). (e) Decoded watermark. (f) Recovered image with EDF inverse halftoning. (g) Recovered image with DBS inverse halftoning. (h) Overall performance.

(a)

(b)

(c)

(d)

(e)

(f)

(g)

PSNR	Decoded Modified Coordination		CDR
EDF 47.75 (dB)	Alteration position	Detected position	99.74 %
DBS 52.30 (dB)	(Nx_s, My_s) = (244, 348) (Nx_e, My_e) = (284, 396)	(Nx_s, My_s) = (248, 352) (Nx_e, My_e) = (288, 400)	

(h)

FIGURE 25. Surveillance application with HRBWE. (a) Original host image. (b) Original watermark. (c) Embedded result. (d) Alterated and detected result (in red). (e) Decoded watermark. (f) Recovered image with EDF inverse halftoning. (g) Recovered image with DBS inverse halftoning. (h) Overall performance.

HRAWE and HRBWE are 0 and 3, respectively. Figures 24(a) and 25(a) show the original host images, and Figures 24(b) and 25(b) show the original watermarks. Figures 24(c) and 25(c) show the embedded results. Figures 24(d) and 25(d) show the alterated and detected result (in red). Figures 24(e)and 25(e) show the decoded watermark. Figures 24(f) and 25(f) show the recovered image with EDF inverse halftoning, while Figures 24(g) and 25(g) show the recovered image with DBS inverse halftoning. Figures 24(h) and 25(h) show the overall performance.

5. **Conclusions.** Nowadays, numerous of watermarking schemes have been created. Most of the methods endeavor to resist more and more attacks, which makes it difficult to look after other issues, such as image quality, complexity, and capacity. This study presents two watermarking schemes, namely Halftone Replacement After Watermark Embedding (HRAWE) and Halftone Replacement Before Watermark Embedding (HRBWE), for medical and surveillance systems. The reason we dedicate on the two applications is their special requirements in practice: The medical system demands high image quality, and the surveillance system requires real-time low complexity and robustness for reasonable compression attack. The watermarking on both applications requires additional capability of alteration region detection and recovery. For these, the HRAWE provides better image quality, while HRBWE provides higher robustness to withstand attacks. Two inverse halftoning approaches, EDF-based and DBS-based, are also proposed to detect alteration region and recover the original image. The EDF-based inverse hlftoning has low complexity advantage. Thus, it is mainly used in cooperating with HRBWE for surveillance images to withstand compression or unauthorized modification. On the other hand, the DBS-based inverse halftoning gears high image quality advantage. Hence, it is mainly used in cooperating with HRAWE for medical images to detect and recover unauthorized modification.

REFERENCES

[1] M. D. Swanson, M. Kobayashi and A. H. Tewfik, Multimedia data-embedding and watermarking technologies, *Proc. of IEEE*, vol.86, no.6, pp.1064-1087, 1998.

[2] M.-M. Yeung and F. Mintzer, An invisible watermarking technique for image verification, *IEEE International Conference on Image Processing*, vol.2, pp.680-683, 1997.

[3] N. Nikolaidis and I. Pitas, Robust image watermarking in the spatial domain, *Signal Processing*, vol.66, no.3, pp.385-403, 1998.

[4] V. Ratnakar, Image watermarking with zero-mean patches, *Conference Record of the Thirty-Third Asilomar Conference on Signals, Systems, and Computers*, vol.2, pp.1513-1517, 1999.

[5] R. G. van Schyndel, A. Z. Tirkel and C. F. Osborne, A digital watermark, *IEEE International Conference on Image Processing*, vol.2, pp.86-90, 1994.

[6] I. Cox, J. Kilian, F. T. Leighton and T. Shamoon, Secure spread spectrum watermarking for multimedia, *IEEE Transactions on Image Processing*, vol.6, no.12, pp.1673-1687, 1997.

[7] W. Zhu, Z. Xiong and Y. Q. Zhang, Multiresolution watermarking for images and video, *IEEE Transactions on Circuits Systems for Video Technology*, vol.9, no.4, pp.545-550, 1999.

[8] C.-T. Hsu and J.-L. Wu, Hidden digital watermarks in images, *IEEE Transactions on Image Processing*, vol.8, no.1, pp.58-68, 1999.

[9] J. Huang, Y.-Q. Shi and Y. Shi, Embedding image watermarks in DC components, *IEEE Transactions on Circuits Systems for Video Technology*, vol.10, no.6, pp.974-979, 2000.

[10] C.-S. Lu, S.-K. Huang, C.-J. Sze and H.-Y. Liao, Cocktail watermarking for digital image protection, *IEEE Transactions on Multimedia*, vol.2, no.4, pp.209-224, 2000.

[11] C. Nafornita, A. Isar and M. Borda, Image watermarking based on the discrete wavelet transform statistical characteristics, *International Conference on Computer as a Tool*, vol.2, pp.943-946, 2005.

[12] C.-S. Lu and H.-Y. Liao, Multipurpose watermarking for image authentication and protection, *IEEE Transactions on Image Processing*, vol.10, no.10, pp.1579-1592, 2001.

[13] F. Khelifi, A. Bouridane, F. Kurugollu and A. I. Thompson, An improved wavelet-based image watermarking technique, *IEEE Conference on Advanced Video and Signal Based Surveillance*, pp.588-592, 2005.
[14] Z. Wang, N. Wang and B. Shi, A novel blind watermarking scheme based on neural network in wavelet domain, *World Congress on Intelligent Control and Automation*, vol.1, pp.3024-3027, 2006.
[15] H. Inoue, A. Miyazaki, A. Yamsmoto and T. Katsura, A digital watermark based on the wavelet transform and its robustness on image compression, *IEEE International Conference on Image Processing*, vol.2, pp.391-395, 1998.
[16] R. Dugad, K. Ratakonda and N. Ahuja, A new wavelet-based scheme for watermarking images, *IEEE International Conference on Image Processing*, vol.2, pp.419-423, 1998.
[17] J. M. Shapiro, Embedded image coding using zerotrees of wavelet coefficients, *IEEE Transactions on See Also Acoustics, Speech, and signal Processing*, vol.41, no.12, pp.3445-3462, 1993.
[18] F. Huo and X. Guo, A wavelet based image watermarking scheme, *IEEE International Conference on Image Processing*, pp.2573-2576, 2006.
[19] V. Solachidis and I. Pitas, Circularly symmetric watermark embedding in 2-D DFT domain, *IEEE Transactions on Image Processing*, vol.6, no.11, pp.1741-1753, 2001.
[20] M. Al-Khassaweneh and S. Aviyente, Spatially adaptive wavelet thresholding for image watermarking, *IEEE International Conference on Multimedia and Expo*, pp.1597-1600, 2006.
[21] R. Ulichney, *Digital Halftoning*, MIT Press, Cambridge, MA, 1987.
[22] J. F. Jarvis, C. N. Judice and W. H. Ninke, A survey of techniques for the display of continuous-tone pictures on bilevel displays, *Computer Graphics and Image Processing*, vol.5, no.1, pp.13-40, 1976.
[23] P. Stucki, MECCA-A multiple-error correcting computation algorithm for bilevel image hardcopy reproduction, *Res. Rep. RZ1060*, IBM Res. Lab., 1981.
[24] L.-D. Li, B.-L. Guo and J.-S. Pan, Robust image watermarking using feature based local invariant regions, *International Journal of Innovative Computing, Information and Control*, vol.4, no.8, pp.1977-1986, 2008.
[25] R. W. Floyd and L. Steinberg, An adaptive algorithm for spatial gray scale, *Proc. of SID 75 Digest. Society for information Display*, pp.36-37, 1975.
[26] V. Ostromoukhov, A simple and efficient error-diffusion algorithm, *Proc. of SIGGRAPH*, pp.567-572, 2001.
[27] D.-L. Lau and G. R. Arce, *Modern Digital Halftoning*, Marcel Dekker, Inc., 2000.
[28] D.-L. Lau and G. R. Arce, Robust halftoning with green-noise, *IS&T's Image Processing, Image Quality, Image Capture Systems Conference*, pp.315-320, 1999.
[29] D.-L. Lau, G. R. Arce and N. C. Gallagher, Green-noise digital halftoning, *Proc. of the IEEE*, vol.86, no.12, pp.2424-2444, 1998.
[30] D.-L. Lau, G. R. Arce and N. C. Gallagher, Digital halftoning via green-noise masks, *Journal of the Optical Society of America*, vol.16, no.7, pp.1575-1586, 1999.
[31] D.-L. Lau, G. R. Arce and N. C. Gallagher, Digital color halftoning with generalized error-diffusion and vector green-noise masks, *IEEE Transactions on Image Processing*, vol.9, no.5, pp.923-935, 2000.
[32] R. Levien, Output dependant feedback in error diffusion halftoning, *IS&T's the 8th International Congress on Advances in Non-Impact Printing Technologies*, pp.280-282, 1992.
[33] D.-L. Lau, G. R. Arce and R. Ulichney, Blue and green noise halftoning models, *IEEE Signal Processing Magazine*, vol.20, no.4, pp.28-38, 2003.
[34] D. E. Knuth, Digital halftones by dot diffusion, *ACM Transaction on Graphics*, vol.6, no.4, 1987.
[35] M. Mese and P. P. Vaidyanathan, Optimized halftoning using dot diffusion and methods for inverse halftoning, *IEEE Transactions on Image Processing*, vol.9, no.4, pp.691-709, 2000.
[36] M. Analoui and J. P. Allebach, Model based halftoning using direct binary search, *Proc. of SPIE, Human Vision, Visual Processing, Digital Display III*, vol.1666, pp.96-108, 1992.
[37] A. Zakhor, S. Lin and F. Eskafi, A new class of B/W and color halftoning algorithm, *IEEE International Conference on Acoustics, Speech and Signal Processing*, vol.4, pp.2801-2804, 1991.
[38] D. Anastassion, Error diffusion coding for A/D conversion, *IEEE Transactions on Circuits and Systems*, vol.36, no.9, pp.1175-1186, 1989.
[39] D. Anastassiou and S. Kollias, Digital image halftoning using neural networks, *Proc. of SPIE*, vol.1001, 1988.
[40] J. B. Mulligan and A. J. Ahumada Jr., Principled halftoning based on models of human vision, *Proc. of SPIE, Human Vision, Visual Processing, Digital Display III*, vol.1666, pp.109-121, 1992.